Multilayer Thin-Film Stacks With Steplike Spatial Beam Shifting

Martina Gerken, *Member, IEEE,* and David A. B. Miller, *Fellow, IEEE, Fellow, OSA*

***Abstract*—This paper demonstrates the use of a single multilayer thin-film stack for generating custom-engineered spatial dispersion, i.e., spatial shift as a function of wavelength. Based on group-velocity effects similar to the superprism effect observed in photonic crystals, this thin-film grating (TFG) device allows for multiplexing or demultiplexing multiple wavelength-division-multiplexed (WDM) channels using a single nonperiodic thin-film stack. We designed a four-channel TFG for coarse WDM applications with 20-nm channel spacing and flat-top passbands. This paper shows that flat-top passbands correspond to a steplike spatial beam shifting with wavelength. The influence of a finite beamwidth on the passband shape is discussed using Fourier decomposition of the beam into plane-wave components. The paper concludes with experimental results for a three-channel TFG demonstrating steplike beam shifting.**

***Index Terms*—Demultiplexing, multiplexing, spatial dispersion, thin-film.**

I. Introduction

LONG-HAUL optical transmission systems use wavelength-division multiplexing (WDM) to increase the data transmission rate by encoding different channels with different wavelengths. Recently, coarse WDM (CWDM) has been emerging in local or metro optical networks. CWDM systems typically have four to 16 channels with channel spacings around 20 nm in the wavelength ranges around 0.8, 1.3, or 1.55 μm. Such systems create a strong need for compact and cost-effective wavelength multiplexing (MUX) and demultiplexing (DEMUX) devices.

MUX/DEMUX devices in current use include diffraction gratings, arrayed-waveguide gratings (AWGs), fiber Bragg gratings (FBGs), and thin-film filters [1]–[3]. Diffraction gratings and AWGs are particularly interesting for high-channel-count systems, as they allow the multiplexing of many channels using a single device. For cost-effective lower channel count systems, thin-film filters or FBGs are typically preferred, due to their lower initial cost and the possibility of upgrading the channel count progressively. FBGs and thin-film filters are 1×2 devices, i.e., they have one input and two outputs. For an n-channel system, $n - 1$ separate devices are needed, leading to cascading losses and a more complex module assembly as the number of channels is increased.

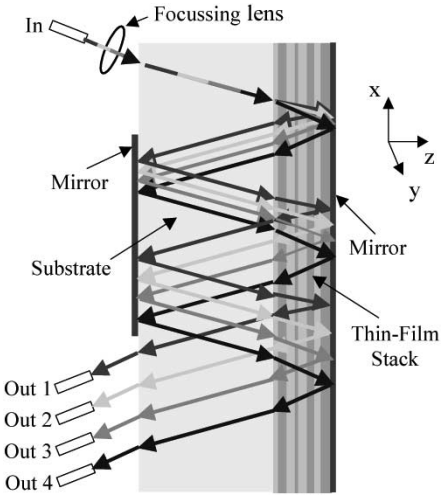

Fig. 1. Schematic of four-channel TFG.

Previously, we suggested the use of group-velocity effects in multilayer thin-film structures to separate multiple beams of different wavelengths by spatial beam shifting, as depicted in Fig. 1 [4], [5]. The thin-film stack is designed such that beams of different wavelengths incident at an angle onto the stack are spatially shifted along the x direction upon reflection. The spatial offset between different wavelengths is increased by performing multiple bounces through the structure. This thin-film grating (TFG) device concept is by no means limited to four channels. Depending on the dispersion characteristics of the multilayer thin-film stack and the beam size, more channels can be multiplexed or demultiplexed. The TFG utilizes well-known thin-film fabrication technology while at the same time eliminating the need to cascade devices, as in the case of traditional thin-film filters. This promises cost reduction, easier assembly, and reduced losses. In this paper, we investigate how to design a TFG with the desired passband-shape characteristics.

II. Steplike Spatial Beam Shifting

The key component of the TFG in Fig. 1 is the thin-film stack with high spatial dispersion, i.e., a large spatial shift in the x direction with wavelength. In [4], we have shown that the photonic crystal "superprism effect" of a periodic dielectric stack results in high spatial dispersion close to the stopband edge and can be used for multiplexing WDM channels. Such a periodic dielectric stack exhibits a nonlinear spatial shift along the x direction

Manuscript received May 2, 2003; revised November 24, 2003. This work was supported by the DARPA Optocenters Program. The work of M. Gerken was supported in part by the Sequoia Capital Stanford Graduate Fellowship.

M. Gerken was with Edward L. Ginzton Laboratory, Stanford University, Stanford, CA 94305 USA. She is now with the University of Karlsruhe, 76131 Karlsruhe, Germany.

D. A. B. Miller is with the Edward L. Ginzton Laboratory, Stanford University, Stanford, CA 94305 USA.

Digital Object Identifier 10.1109/JLT.2004.824380

0733-8724/04$20.00 © 2004 IEEE

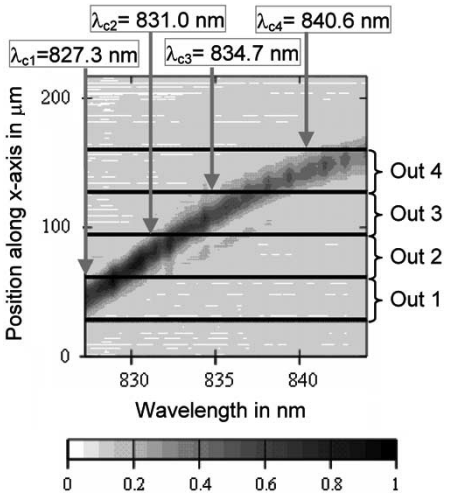

Fig. 2. Experimental intensity (linear scale, arbitrary units) as a function of position and wavelength for eight bounces off a 66-layer nonperiodic stack at 54° incidence angle and p-polarization.

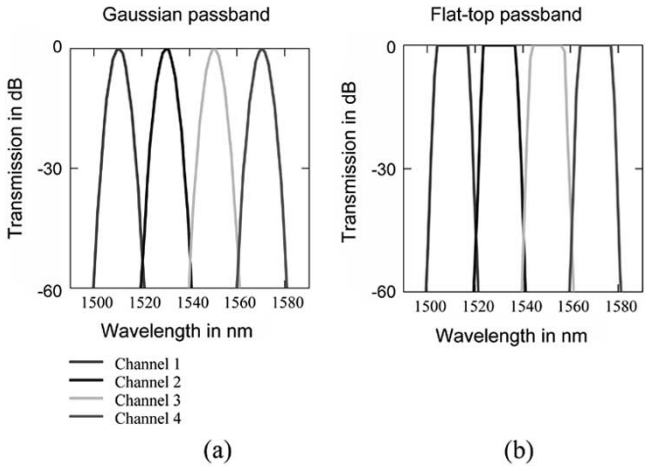

Fig. 3. Schematic of (a) a Gaussian passband shape compared with (b) a flat-top passband shape (transmission refers to the energy transfer from input to output).

with wavelength. Therefore, if the outputs Out 1, Out 2, Out 3, and Out 4 in Fig. 1 are equally spaced, the channel spacing cannot be equal in wavelength.

In order to obtain equal channel spacing, we investigated the design of nonperiodic thin-film stacks exhibiting a linear shift with wavelength and thus constant dispersion [5], [6]. Fig. 2 plots the beam intensity as a function of position and wavelength for eight bounces off a nonperiodic 66-layer stack. The stack composition is given as Design L in Appendix C. These are experimental results for a 54° incidence angle and p-polarization. Due to the oblique incidence angle, this device is polarization sensitive and only works for p-polarization. The intensity decreases with wavelength as the stack itself is more transmissive for longer wavelengths, and the mirror on the stack side shown in Fig. 1 was not applied. Fig. 2 shows that this device exhibits a total shift of approximately 100 μm and can separate four wavelength channels by their Gaussian beamwidths [6].

The center wavelengths λ_{c1} to λ_{c4} of the different channels are indicated in the figure. The horizontal lines represent the spatial boundaries between channels. Since the beam shifts linearly with wavelength, the beam has a different center position for each wavelength. Thus, only the center wavelength λ_{ci} of the ith channel is exactly centered on Out i. If the channel drifts to an off-center wavelength, the beam position changes, and the coupling efficiency to Out i is reduced. In the case of a Gaussian beam profile, the passband shape is also Gaussian for a device with constant dispersion.

A theoretical Gaussian passband shape is depicted in Fig. 3(a). For practical WDM systems, we ideally want a flat-top passband shape, as shown in Fig. 3(b). This allows for a drift in the channel wavelength without incurring loss. In order to obtain a flat-top passband shape, we need to design a steplike shift with wavelength. Such a steplike shift results in a range of wavelengths to be shifted to the same exit position. Therefore, if the output is located at this position, there will be no loss for any wavelength within the range.

A TFG exhibiting a steplike shift with wavelength can be designed employing methods similar to the ones described in [5]. Numerical refinement [7] is used to gradually improve the performance of a start design until the structure matches the desired characteristics sufficiently well. To prevent reflections off the interface between the substrate and the thin-film stack, we use a "tapered" Bragg stack as the start design [8]. In such a Bragg stack, the periodicity is slowly "turned on" by increasing the amount of high-index material in each period. The desired dispersion characteristics were solely obtained using numerical refinement. We also tried analytical coupled-cavity design techniques [2], [9] but did not achieve good results due to the large number of cavities needed to approximate a steplike function.

Using numerical optimization, we designed a four-channel flat-top TFG with 20-nm wavelength spacing and channel center wavelengths at 1510, 1530, 1550, and 1570 nm, which is particularly well suited for CWDM systems [10]. The design has 100 alternating layers of SiO_2 $(n = 1.46)$ and Ta_2O_5 $(n = 2.06)$ with a total stack thickness of 33.1 μm. The stack is designed for operation through a quartz $(n = 1.52)$ substrate at 45° incidence angle and p-polarization. Only the first 80 layers were modified during refinement to obtain the desired dispersion characteristics. The last 20 layers were fixed as a Bragg stack to achieve high reflectance. The lowest reflectance is 96% after a single bounce, corresponding to a maximum intrinsic loss of 28% after eight bounces assuming a 100% mirror on the substrate side. More periods could be used to further decrease the loss due to transmission. This device likely has negligible absorption loss. The stack composition is given as Design S in Appendix C. Fig. 4 plots the theoretical performance of the four-channel design obtained using a plane-wave transfer matrix calculation [5]. The steplike shift as a function of wavelength is clearly visible in Fig. 4(a).

III. Influence of the Finite Beamwidth

As seen in Fig. 1, we need to focus the incident beam to spatially separate beams of different wavelengths. For a smaller Gaussian spot size of the focussed beams, less spatial shift is necessary for demultiplexing. Next, we will investigate the influence of the beamwidth on the spatial shift with wavelength.

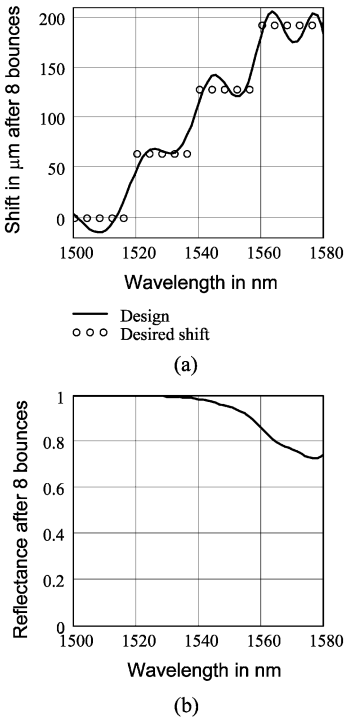

Fig. 4. CWDM four-channel TFG. (a) Theoretical shift and (b) reflectance after eight bounces off the 100-layer stack at 45° incidence angle and p-polarization (plane-wave calculation).

Appendix A discusses how a beam can be decomposed into plane waves with different incidence angles. Only a limited range of these angular components has a significant intensity. Thus, the input angular range of $\pm\Delta\theta$ can be approximated by the drop of the intensity to $1/\mathrm{e}^2$ as given in

$$\Delta\theta \approx \frac{\lambda}{\pi w_0}. \tag{1}$$

θ is the incidence angle in vacuum, λ is the incident wavelength in vacuum, and w_0 is the Gaussian spot size, i.e., the beam radius. Equation (1) shows that a smaller spot size w_0 corresponds to a larger angular range $\Delta\theta$. Since the spatial shift is a function of the incidence angle and the wavelength (and the polarization), different components of a beam of finite width will incur a different spatial shift. This can potentially lead to beam distortions, and the effect is more severe for beams with a larger range of angular components, i.e., beams with a smaller Gaussian spot size. To investigate the influence of the change in incidence angle on the spatial shift, Fig. 5 plots the shift as a function of wavelength for incidence angles of 44.4°, 45°, and 45.6°. From (1), we find that a $\pm 0.6^\circ$ angular range corresponds to the $1/\mathrm{e}^2$-intensity width of a Gaussian beam with a 50-μm spot size.

Fig. 5 shows that a change in the incidence angle shifts the curve while approximately maintaining the curve shape. In regions of constant dispersion, i.e., where the shift is linear or constant with wavelength, such a shift in the curve corresponds to a change in the focal length but does not distort the beam. If, on the other hand, the dispersion is not constant, beam distortions occur as different angular components of the beam have different focal lengths. We conclude that beam distortions will

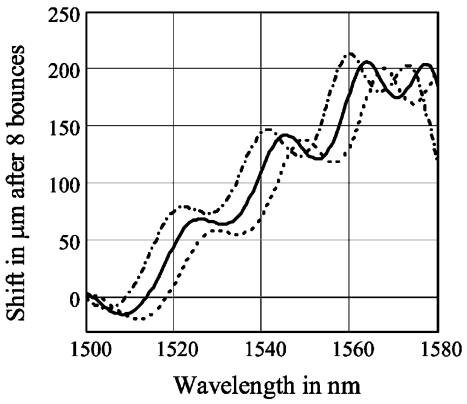

Fig. 5. Shift as a function of wavelength for incidence angles of 44.4° (dotted), 45° (solid), and 45.6° (dashed–dotted).

TABLE I
RELATIONSHIP BETWEEN SPOT SIZE, ANGULAR RANGE, AND WAVELENGTH RANGE AT 1540 nm, 45° INCIDENCE ANGLE, AND $v_{gx} = 0.3c$

Spot Size w_0	Angular Range $\Delta\theta$	Wavelength Range $\Delta\lambda$
15 μm	1.9°	14 nm
30 μm	0.9°	7 nm
50 μm	0.6°	4 nm

be minimal, as long as all relevant angular components of a finite-width beam see the same dispersion, which corresponds in the case of a step design to all components being on the same "step." From Fig. 5, it follows that at the short-wavelength edge of a "step," angular components with a smaller incidence angle already experience the shift of the next lower "step," and similarly, at the long-wavelength edge, larger incidence angle components already see the next higher "step." Therefore, the useful wavelength range of a "step" is limited by the beamwidth. We see that a beam of finite width essentially probes the spatial shift over a range of wavelengths.

To quickly approximate the behavior of a designed structure for different beamwidths, we find the following approximation useful:

$$\Delta\lambda \approx \frac{-\lambda\cos\theta}{\sin\theta - c/v_{gx}}\Delta\theta. \tag{2}$$

This equation relates the change in the incidence angle $\Delta\theta$ to the shift of the curve in wavelength $\Delta\lambda$. c is the speed of light in vacuum, and v_{gx} is the group velocity in the x direction. (Appendix B provides more background on this approximation.) We have discussed previously that the group velocity v_{gx} along the layers is approximately constant for many structures of interest [5]. Therefore, the proportionality factor in (2) is approximately constant, and the "probed" wavelength range is proportional to the angular range of the beam. Table I gives three examples of the relationship between spot size, angular range, and wavelength range. The group velocity v_{gx} is set to 0.3 times the speed of light.

From Table I, we see that for a beam with a spot size of 50 μm, the different beam components probe approximately ± 4 nm of the design around the incident wavelength. Remember that the incident light is assumed to be monochromatic and that this

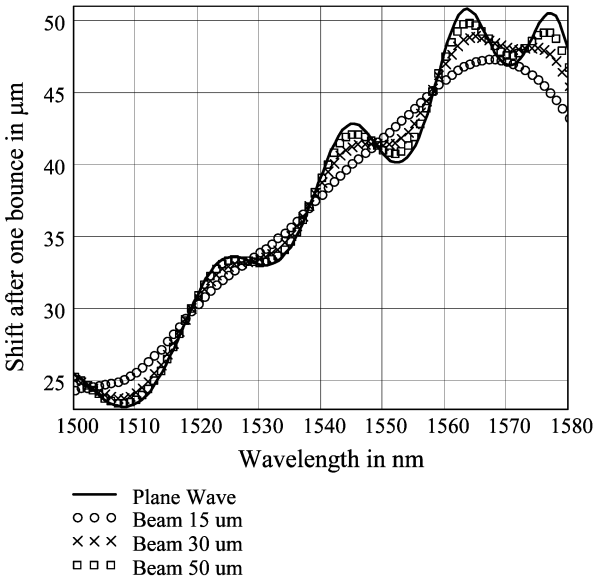

Fig. 6. Shift as a function of wavelength at 45° incidence angle for a plane wave and Gaussian beams with 15-, 30-, and 50-μm spot size.

probing is due to the different angular components. As the design in Fig. 4 is quite flat over a $\pm$4-nm wavelength range around the channel center wavelengths, we expect all angular components of 50-μm beams to see the same spatial dispersion. Toward the edge of the band of zero dispersion, the beams will become broadened, however, as some of the angular components see a different spatial dispersion. Therefore, the whole range that is flat for the plane-wave calculation in Fig. 4 may not be usable for beams of finite size.

As a 50-μm beam probes a $\pm$4-nm wavelength range, features smaller than this wavelength range will be averaged out. For a 15-μm beam, features smaller than $\pm$14 nm will be averaged out. Considering this, we cannot expect the design in Fig. 4 to work well with a 15-μm beam. To model the propagation of a beam of finite width through the device, we use the Fourier decomposition technique described in Appendix A. Each plane-wave component of the beam is propagated separately through the thin-film stack, and the resulting output beam is obtained by summing the individual components. The center position of the beam is obtained by performing a Gaussian beam fit varying the beam amplitude, center position, and width. Fig. 6 plots the shift of the beam center position as a function of wavelength for incident plane waves and three different beam sizes. Indeed we see that for a 15-μm incident beam, the steplike shift is completely averaged out, while it is clearly visible for the 30- and 50-μm beam size. This shows explicitly that in designing a TFG with a steplike shift, we have to take care to use a sufficiently large spot size.

IV. Experimental Results

The four-channel CWDM design shown in Fig. 4 is not yet fabricated, but we have performed preliminary experiments demonstrating a three-channel steplike spatial beam shifting. The 66-layer stack (Design L in Appendix C) discussed in Fig. 2 exhibits a steplike beam shifting for a 48° incidence angle. Fig. 7(a) shows the experimentally measured intensity

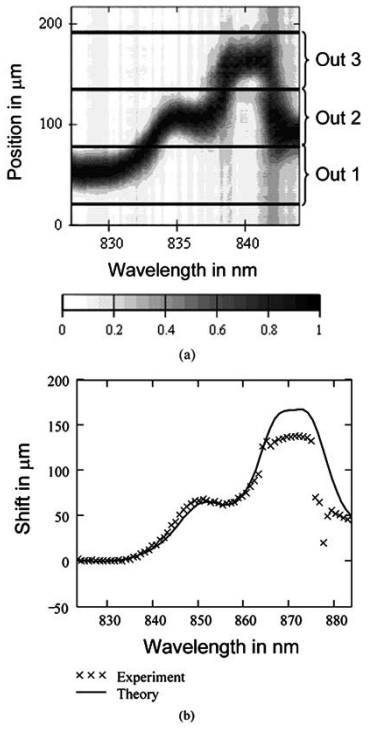

Fig. 7. Three-channel TFG. (a) Experimentally obtained intensity (linear scale) as a function of position and wavelength for eight bounces off a 66-layer stack at 48° incidence angle and p-polarization. Peak intensity is normalized to unity for each wavelength. (b) Comparison between experiment and plane-wave theory.

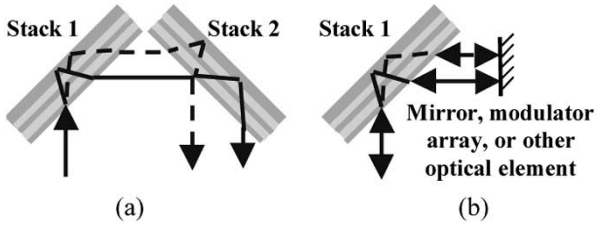

Fig. 8. Systems using stacks with high spatial dispersion. (a) Combination of two stacks with opposite dispersion can be used to obtain spatial dispersion without temporal dispersion. (b) System providing temporal dispersion without spatial dispersion. This system could also be used to manipulate channels of different wavelengths independently.

as a function of position and wavelength for eight bounces at 48° incidence angle, p-polarization, and an incident beam size of 18 μm. The intensity at each wavelength is normalized to unity, as this structure was not designed for high reflectance at 48° and shows significant loss. Nevertheless, the agreement between the experimentally observed shift and the theoretically expected shift as seen in Fig. 7(b) is promising. The steplike spatial shift is clearly visible, and after eight bounces, the steps are sufficiently high to separate the different channels by their beamwidth.

V. Separating Spatial and Temporal Dispersion

As discussed in [5], stacks with spatial dispersion exhibit temporal dispersion at the same time. For short-pulse operation, it may be important to eliminate this temporal dispersion. Fig. 8(a) shows how a combination of two stacks with opposite dispersion can be used in series to cancel the temporal dispersion while

doubling the spatial dispersion. This would require the design of a second structure with opposite dispersion. On the other hand, backreflection through the same stack can be used if a system with temporal dispersion (but no spatial dispersion) is desired, as shown in Fig. 8(b). Replacing the mirror by a modulator array or another optical element, the different wavelength components can be modulated independently. This system can easily be extended to a two-dimensional array by using the y dimension perpendicular to the plane of the page. This concept is applicable to both the step dispersion discussed in this paper and also the other forms of dispersion (linear and nonlinear) discussed previously.

VI. Conclusion

In conclusion, we demonstrated how a single thin-film stack with high spatial dispersion can be used to multiplex or demultiplex multiple wavelength channels. We explained that a linear spatial shift with wavelength corresponds to a Gaussian passband shape. In order to obtain a more desirable flat-top passband shape, we designed thin-film stacks exhibiting a steplike spatial shift with wavelength. We discussed the influence of a finite beamwidth on the device performance.

This TFG device is particularly interesting for CWDM applications as it can be fabricated cost-effectively using well-known thin-film filter fabrication technology. Furthermore, it eliminates the need to cascade multiple devices as in the case of thin-film filters and FBGs, promising an easy and compact module assembly. TFGs are also interesting for any application requiring compact dispersive elements. We have demonstrated that the dispersion characteristics of a multilayer thin-film stack can be designed flexibly to fit the given requirements. Other dispersion profiles besides a linear or a steplike shift as a function of wavelength can be easily generated.

Appendix A
Simulating Beams of Finite Width by Fourier Decomposition

Here we discuss how the propagation of finite-width beams through a thin-film stack can be calculated using a Fourier decomposition technique [11]. The thin-film stack is considered as a system that propagates an input field $E(x_{\rm in}, y_{\rm in}, z_{\rm in})$ from an input position $z = z_{\rm in}$ to an output position $z = z_{\rm out}$. If the reflection of a beam off a thin-film stack is considered, the input and the output positions coincide, and the incident field $E(x_{\rm in}, y_{\rm in}, z_0)$ is given by the forward-propagating beam, while the output field $E(x_{\rm out}, y_{\rm out}, z_0)$ is the reflected beam. The task is to calculate the output field at any output position for an arbitrary input field and an arbitrary stack.

For linear space-invariant systems, the incident field can be decomposed into elementary components; these can be propagated individually, and the output field is obtained by summing the propagated individual components. For sufficiently small intensities, a thin-film stack is a linear system. Furthermore, it is space invariant, since the z direction transfer function only depends on the difference between the input position $(x_{\rm in}, y_{\rm in})$ and the exit position $(x_{\rm out}, y_{\rm out})$, not on the absolute position along the stack. We limit ourselves here to propagation of the beam in the x–z plane and assume that the beam is not focused in the y direction. As seen from Fig. 1, such an elongated beam shape does not reduce the device functionality, and it prevents mixing of the different polarization components.

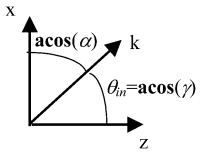

Fig. 9. Direction cosines α and γ for propagation in the x–z plane. k is the wave vector.

One possible decomposition of the incident field $E(x, z = 0)$ is obtained by performing the spatial Fourier transform given by [11]

$$A_{Fx}(f_x; z = 0) = \int_{-\infty}^{\infty} E(x, z = 0) \exp(-i2\pi f_x x) dx. \quad (3)$$

The inverse Fourier transform expresses the field as a function of the Fourier components $A_{Fx}(f_x; z = 0)$, as follows:

$$E(x, z = 0) = \int_{-\infty}^{\infty} A_{Fx}(f_x; z = 0) \exp(i2\pi f_x x) df_x. \quad (4)$$

From the integrand of (4), we see that the Fourier transform decomposes the E-field into plane waves with amplitudes $A_{Fx}(f_x; z = 0)$ and wave vectors $k_x = 2\pi f_x$ in the x direction. The spatial frequency f_x is related to the directional cosine α depicted in Fig. 9 by

$$f_x = \frac{\alpha}{\lambda}. \quad (5)$$

Thus, we see that the integration in (4) corresponds to the summation of plane waves with amplitudes $A_{Fx}(f_x; z = 0)$ propagating in different directions in the x–z plane. We can calculate the plane-wave amplitudes $A_{Fx}(f_x; z)$ as a function of z using e.g., a transfer matrix method [5]. The transfer function relating $A_{Fx}(f_x; z)$ to $A_{Fx}(f_x; 0)$ is called $H(f_x; z)$, as shown in

$$A_{Fx}(f_x; z) = H(f_x; z) A_{Fx}(f_x; 0). \quad (6)$$

Therefore, we can now calculate $E(x, z)$ at any point in the x–z plane by propagating the individual Fourier components and summing them up after propagation as given in

$$\begin{aligned} E(x, z) &= \int_{-\infty}^{\infty} A_{Fx}(f_x; z) \exp(i2\pi f_x x) df_x \\ &= \int_{-\infty}^{\infty} A_{Fx}\left(\frac{\alpha}{\lambda}; z\right) \exp\left(i\frac{2\pi}{\lambda}\alpha x\right) d\frac{\alpha}{\lambda}. \end{aligned} \quad (7)$$

For practical purposes, we will replace the continuous Fourier transform in (7) by a discrete Fourier transform, as shown in (8),

where α_i is the directional cosine of the ith component, and $\Delta\alpha$ is the angular separation of the different components.

$$E(x,z)=\sum_i A_{Fx}\left(\frac{\alpha_i}{\lambda};z\right)\exp\left(\mathrm{i}\frac{2\pi}{\lambda}\alpha_i x\right)\frac{\Delta\alpha}{\lambda}. \quad (8)$$

Due to the discrete nature of the Fourier transform (8), the resulting E-field is repetitive in space. The repetition distance Δx is given by

$$\Delta x=\frac{\lambda}{\Delta\alpha}. \quad (9)$$

If the E-field of interest is limited in space or can be approximated by a spatially limited function extending over a spatial distance smaller than Δx, the discrete Fourier transform (8) combined with a spatial filter of width Δx correctly reconstructs the original field. Solving (9) for $\Delta\alpha$, we obtain the minimum required angular sampling distance. This is the Whittaker–Shannon sampling theorem well known from information theory [11], [12].

Equation (10) gives the field at the beam waist for a beam propagating at an angle θ_{in} with respect to the z axis with a Gaussian field distribution perpendicular to the direction of propagation in the x–z plane. w_0 is the spot size, and E_0 is the E-field amplitude.

$$E_{\mathrm{GB}}(x,z=0)=E_0\exp\left(-\frac{x^2}{(w_0/\cos(\theta_{\mathrm{in}}))^2}\right)\times\exp\left(\mathrm{i}\frac{2\pi}{\lambda}\sin(\theta_{\mathrm{in}})x\right). \quad (10)$$

The Fourier components of this beam are given by

$$A_{Fx\mathrm{GB}}\left(\frac{\alpha}{\lambda};z=0\right)=E_0\frac{w_0}{\cos(\theta_{\mathrm{in}})}\sqrt{\pi}\times\exp\left(-\left(\frac{w_0}{\cos(\theta_{\mathrm{in}})}\right)^2\pi^2\left(\frac{\alpha-\sin(\theta_{\mathrm{in}})}{\lambda}\right)^2\right). \quad (11)$$

Substituting (6) and (11) into (8), we can calculate the E-field at any position in the thin-film stack for an incident Gaussian beam. Remember that this beam is not a true Gaussian beam as we did not consider the beam focusing in the y direction. Instead, here we are modeling a beam with a Gaussian field distribution in the plane of propagation and an infinite width in the y direction. This analysis can be extended to the general case following [11].

Appendix B
Relationship Between a Change in Incidence Angle $\Delta\theta$ and a Change in Incidence Wavelength $\Delta\lambda$

The wave vector K in the z direction, the wave vector β in the x direction, and the frequency ω are related by the dispersion relation [5]. Let us assume that we have the dispersion relation given in the implicit form

$$f(K,\beta,\omega)=0. \quad (12)$$

β and ω are related to θ and λ as given in

$$\beta=\frac{2\pi}{\lambda}\sin(\theta) \quad (13)$$

$$\omega=\frac{2\pi c}{\lambda}. \quad (14)$$

Performing a variable transformation from (β,ω) to (θ,λ), the partial derivatives of the dispersion relation with respect to θ and λ are given by

$$\frac{\partial f}{\partial\theta}=\frac{\partial f}{\partial\beta}\frac{\partial\beta}{\partial\theta}+\frac{\partial f}{\partial\omega}\frac{\partial\omega}{\partial\theta}=\frac{\partial f}{\partial\beta}\frac{2\pi}{\lambda}\cos(\theta) \quad (15)$$

$$\frac{\partial f}{\partial\lambda}=\frac{\partial f}{\partial\beta}\frac{\partial\beta}{\partial\lambda}+\frac{\partial f}{\partial\omega}\frac{\partial\omega}{\partial\lambda}=\frac{\partial f}{\partial\beta}\left(-\frac{2\pi}{\lambda^2}\right)\sin(\theta)+\frac{\partial f}{\partial\omega}\left(-\frac{2\pi c}{\lambda^2}\right). \quad (16)$$

Finally, the partial derivative relating $\partial\theta$ and $\partial\lambda$ is calculated in [13]

$$\left.\frac{\partial\lambda}{\partial\theta}\right|_{K=\mathrm{const}}=-\frac{\partial f/\partial\theta}{\partial f/\partial\lambda}=\frac{\lambda\cos\theta}{\sin\theta-\left.\frac{\partial\beta}{\partial\omega}\right|_{K=\mathrm{const}}c}. \quad (17)$$

$\partial\omega/\partial\beta$ is the group velocity in the x direction v_{gx}. Approximating differences by differentials, we obtain the relationship between a change in incidence angle $\Delta\theta$ and a change in incidence wavelength $\Delta\lambda$ as given in (2). Note that the sign in (17) is different since we consider in (2) the shift of the curve, not a change in the incidence wavelength. Also note that the partial derivative in (17) is not for a constant beam shift, but for a constant wave vector K. Nevertheless, we found (2) a very useful approximation for estimating the behavior of the shift with wavelength for a change in the incidence angle $\Delta\theta$.

TABLE II
COMPOSITION OF DESIGNS

		Design L	Design S		Design L	Design S
Material	Layer #	Physical Thickness in nm		Layer #	Physical Thickness in nm	
Substrate		Quartz	Quartz			
Ta2O5	1	188.0	404.8	51	89.0	124.6
SiO2	2	276.6	656.8	52	171.6	362.6
Ta2O5	3	188.0	837.2	53	93.0	130.5
SiO2	4	276.6	643.9	54	196.6	307.2
Ta2O5	5	188.0	439.5	55	98.0	136.3
SiO2	6	276.6	672.6	56	164.3	365.6
Ta2O5	7	208.0	492.8	57	98.0	142.2
SiO2	8	380.6	673.5	58	144.6	345.6
Ta2O5	9	194.0	456.9	59	98.0	148.1
SiO2	10	380.6	556.9	60	205.9	347.6
Ta2O5	11	218.0	418.2	61	98.0	154.0
SiO2	12	320.3	531.8	62	197.6	317.6
Ta2O5	13	250.0	357.3	63	109.0	160.0
SiO2	14	295.4	576.5	64	175.8	308.6
Ta2O5	15	278.0	409.2	65	104.0	165.9
SiO2	16	276.6	462.0	66	57.2	299.5
Ta2O5	17	453.0	404.8	67		171.9
SiO2	18	286.0	560.1	68		290.5
Ta2O5	19	453.0	420.4	69		177.9
SiO2	20	263.1	462.1	70		281.4
Ta2O5	21	235.0	416.0	71		177.9
SiO2	22	311.0	504.3	72		248.3
Ta2O5	23	245.0	441.7	73		177.9
SiO2	24	289.1	485.7	74		281.5
Ta2O5	25	249.0	437.4	75		178.0
SiO2	26	276.6	408.3	76		291.5
Ta2O5	27	254.0	453.0	77		178.0
SiO2	28	262.1	453.0	78		248.2
Ta2O5	29	258.0	457.7	79		178.0
SiO2	30	257.9	432.0	80		305.7
Ta2O5	31	263.0	475.4	81		200.3
SiO2	32	251.7	392.5	82		304.5
Ta2O5	33	60.0	491.1	83		200.3
SiO2	34	241.3	463.2	84		304.5
Ta2O5	35	58.0	475.9	85		200.3
SiO2	36	228.8	387.1	86		304.5
Ta2O5	37	57.0	83.8	87		200.3
SiO2	38	221.5	415.1	88		304.5
Ta2O5	39	61.0	89.6	89		200.3
SiO2	40	219.4	405.9	90		304.5
Ta2O5	41	66.0	95.5	91		200.3
SiO2	42	207.0	393.8	92		304.5
Ta2O5	43	70.0	101.9	93		200.3
SiO2	44	199.7	409.3	94		304.5
Ta2O5	45	75.0	107.1	95		200.3
SiO2	46	198.6	422.5	96		304.5
Ta2O5	47	80.0	113.0	97		200.3
SiO2	48	185.1	334.1	98		304.5
Ta2O5	49	84.0	118.8	99		200.3
SiO2	50	163.3	371.1	100		304.5

APPENDIX C
COMPOSITION OF DESIGNS

The composition of designs is shown in Table II.

ACKNOWLEDGMENT

The authors would like to thank A. Clark of JDS Uniphase for the growth of the sample.

REFERENCES

[1] R. Ramaswami and K. N. Sivarajan, *Optical Networks: A Practical Perspective*. San Mateo, CA: Morgan Kaufmann, 1998.

[2] C. K. Madsen and J. H. Zhao, *Optical Filter Design and Analysis—A Signal Processing Approach*. New York: Wiley, 1999.

[3] H. A. MacLeod, *Thin-Film Optical Filters*. Bristol, U.K.: Institute of Physics, 2001.

[4] B. E. Nelson, M. Gerken, D. A. B. Miller, R. Piestun, C.-C. Lin, and J. S. Harris, Jr., "Use of a dielectric stack as a one-dimensional photonic crystal for wavelength demultiplexing by beam shifting," *Opt. Lett.*, vol. 25, no. 20, pp. 1502–1504, 2000.

[5] M. Gerken and D. A. B. Miller, "Multilayer thin-film structures with high spatial dispersion," *Appl. Opt.*, vol. 42, no. 7, pp. 1330–1345, 2003.

[6] ——, "Wavelength demultiplexer using the spatial dispersion of multilayer thin-film structures," *IEEE Photon. Technol. Lett.*, vol. 15, pp. 1097–1099, Aug. 2003.

[7] J. A. Dobrowolski and R. A. Kemp, "Refinement of optical multilayer systems with different optimization procedures," *Appl. Opt.*, vol. 29, no. 19, pp. 2876–2893, 1990. and refs. herein.

[8] N. Matuschek, F. X. Kärtner, and U. Keller, "Theory of double-chirped mirrors," *IEEE J. Select. Topics Quantum Electron.*, vol. 4, pp. 197–208, Apr. 1998.

[9] M. Jablonski, Y. Takushima, and K. Kikuchi, "The realization of all-pass filters for third-order dispersion compensation in ultrafast optical fiber transmission systems," *J. Lightwave Technol.*, vol. 19, pp. 1194–1205, Aug. 2001.

[10] M. Gerken and D. A. B. Miller, "Thin-film (DE)MUX based on step-like spatial beam shifting," presented at the IEEE LEOS 2002 Annu. Meeting, Glasgow, U.K., Nov. 10–14, 2002. Paper ThV 3.

[11] J. W. Goodman, *Introduction to Fourier Optics*. New York: McGraw-Hill, 1996.

[12] A. V. Oppenheim, R. W. Schafer, and J. R. Buck, *Discrete-Time Signal Processing*. Englewood Cliffs, NJ: Prentice-Hall, 1999.

[13] I. N. Bronstein, K. A. Semendjajew, G. Musiol, and H. Muehlig, "Verlag Harri Deutsch, Thun und Frankfurt am Main," *Taschenbuch Math.*, pp. 232–237, 1993.

Martina Gerken (S'00–M'04) received the Dipl.-Ing. degree in electrical engineering from the University of Karlsruhe, Germany, in 1998 and the Ph.D. degree in electrical engineering from Stanford University, Stanford, CA, in 2003.

She worked on optical measurement systems under Dr. G. Faris at SRI International, Menlo Park, CA, in 1998 and 1999. From 1999 to 2003, she performed her Ph.D. research on dispersive nanostructures for wavelength multiplexing under Prof. D. A. B. Miller at Stanford University. Currently, she holds a position at the University of Karlsruhe, working in the group of Prof. U. Lemmer on periodic and nonperiodic photonic nanostructures.

David A. B. Miller (M'84–SM'89–F'95) received the B.Sc. degree from St. Andrews University, St. Andrews, U.K., and the Ph.D. degree from Heriot–Watt University, Edinburgh, U.K., in 1979.

He worked at Bell Laboratories from 1981 to 1996 and was a Department Head since 1987, latterly of the Advanced Photonics Research Department. He is currently the W. M. Keck Foundation Professor of Electrical Engineering at Stanford University, Stanford, CA, and Director of the Ginzton and Solid State and Photonics Laboratories. His research interests include quantum-well optoelectronic physics and devices and fundamentals and applications of optics in information, sensing, switching, and processing. He has published more than 200 scientific papers and holds more than 50 patents.

Dr. Miller is a Fellow of the Royal Societies of London and Edinburgh, the Optical Society of America (OSA), and the American Physical Society (APS). He has served as a Board Member for both OSA, the IEEE Lasers and Electro-Optics Society (LEOS), and various other Society and conference committees. He was President of the IEEE LEOS in 1995. He was awarded the Adolph Lomb Medal and R. W. Wood Prize from OSA, the International Prize in Optics from the International Commission for Optics, and an IEEE Third Millennium Medal and holds honorary degrees from the Vrije Universiteit Brussel and Heriot–Watt University.